

Inert Doublet Dark Matter with Strong Electroweak Phase Transition

Debasish Borah*

Department of Physics, Indian Institute of Technology Bombay, Mumbai - 400076, India

James M. Cline†

Department of Physics, McGill University, 3600 Rue University, Montréal, Québec, Canada H3A 2T8

We reconsider the strength of the electroweak phase transition (EWPT) in the inert doublet dark matter model, using a quantitatively accurate form for the one-loop finite temperature effective potential, taking into account relevant particle physics and dark matter constraints, focusing on a standard model Higgs mass near 126 GeV, and doing a full scan of the space of otherwise unconstrained couplings. We find that there is a significant (although fine-tuned) space of parameters for achieving an EWPT sufficiently strong for baryogenesis while satisfying the XENON100 constraints from direct detection and not exceeding the correct thermal relic density. We predict that the dark matter mass should be in the range 60 – 67 GeV, and we discuss possible LHC signatures of the charged and CP-odd Higgs bosons, including a $\sim 10\%$ reduction of the $h \rightarrow \gamma\gamma$ branching ratio.

1. INTRODUCTION

Models of scalar dark matter (DM) H can have interesting connections to Higgs boson (h) physics because of the dimension 4 operator $|h|^2|H|^2$. One obvious consequence is the possibility of the invisible decay channel $h \rightarrow HH$ if the dark matter is sufficiently light. Another is that such a coupling can allow the electroweak phase transition (EWPT) to become first order, and potentially strong enough to be interesting for baryogenesis [1]. There has been considerable interest in the interplay between dark matter and the electroweak phase transition in recent years [2]-[10].

The Inert Doublet Model (IDM) is a widely studied setting for scalar dark matter [11–14] that can have rich phenomenological consequences [15]-[26]. Recently its capacity for giving a strong EWPT was considered by ref. [27]. That work found a rather large allowed region of parameter space where the EWPT could be strong and other constraints satisfied, including the correct thermal relic DM density. However, it employed a simplified version of the finite-temperature effective potential, keeping only terms up to $O(m/T)^3$ in the high-temperature expansion. On the other hand, a very quantitative treatment of the effective potential for two-Higgs doublet models was recently undertaken in ref. [28]. Our purpose in this paper is to reexamine the strength of the EWPT in the IDM using this more accurate potential. Moreover we search the full parameter space of the model using Monte Carlo methods, rather than a restricted subspace using a grid search as was done in [27]. We also focus on values of the standard model-like Higgs boson mass near 126 GeV, the value favored by recent LHC data [29]-[32].

In this way we are able to extend the results of [27], confirming that there exists a significant (though finely

tuned) region of parameter space in the IDM where the strength of the EWPT is sufficiently enhanced for electroweak baryogenesis while satisfying other necessary constraints. The paper is structured as follows. We review the definition of the model and collider mass constraints in section 2, our methodology for defining the effective potential and scanning the parameter space in section 3, and we present the results of the Monte Carlo search in section 4. Prospects for testing the model at colliders are discussed in section 5, and we give conclusions in section 6.

2. THE INERT DOUBLET MODEL

The Inert Doublet Model is the extension of the standard model (SM) by an additional Higgs doublet S with the discrete Z_2 symmetry $S \rightarrow -S$, which naturally leads to a stable dark matter candidate in one of the components of S [12, 14, 33]. Since an unbroken Z_2 symmetry forbids Yukawa couplings involving S , the second doublet interacts with the SM fields only through its couplings to the SM Higgs doublet and the gauge bosons. The scalar potential of the IDM is given by

$$\begin{aligned} V = & \frac{\lambda}{4} \left(H^{\dagger i} H_i - \frac{v^2}{2} \right)^2 + m_1^2 (S^{\dagger i} S_i) \\ & + \lambda_1 (H^{\dagger i} H_i) (S^{\dagger j} S_j) + \lambda_2 (H^{\dagger i} H_j) (S^{\dagger j} S_i) \\ & + [\lambda_3 H^{\dagger i} H^{\dagger j} S_i S_j + \text{h.c.}] + \lambda_S (S^{\dagger i} S_i)^2 \end{aligned} \quad (1)$$

We assume that S does not acquire a vacuum expectation value (VEV), so as to keep the Z_2 symmetry unbroken. The tree-level scalar mass eigenvalues are

$$\begin{aligned} m_h^2 &= \frac{1}{2} \lambda v^2 \\ m_H^2 &= m_1^2 + \frac{1}{2} (\lambda_1 + \lambda_2 + 2\lambda_3) v^2 \\ m_A^2 &= m_1^2 + \frac{1}{2} (\lambda_1 + \lambda_2 - 2\lambda_3) v^2 \\ m_{\pm}^2 &= m_1^2 + \frac{1}{2} \lambda_1 v^2 \end{aligned} \quad (2)$$

*Electronic address: debasish@phy.iitb.ac.in

†Electronic address: jcline@physics.mcgill.ca

where m_h is the SM-like Higgs mass, m_H (m_A) is the mass of CP-even (odd) component of the inert doublet, and m_{\pm} is the mass of the charged Higgs. Without loss of generality, we can take $\lambda_3 < 0$ so that $m_H < m_A$ and therefore H is the dark matter particle. The case $\lambda_3 > 0$ just corresponds to renaming $H \leftrightarrow A$. We further restrict $\lambda_2 + 2\lambda_3 < 0$ so that $m_H < m_{\pm}$ to avoid the charged state being dark matter.

2.1. Collider Mass Bounds

Precision measurement of the Z boson decay width at LEP I forbids the Z boson decay channel $Z \rightarrow HA$, which requires that $m_H + m_A > m_Z$. In addition, LEP II constraints roughly rule out the triangular region [34]

$$m_H < 80 \text{ GeV}, \quad m_A < 100 \text{ GeV}, \quad m_A - m_H > 8 \text{ GeV}$$

We take the lower bound on the charged scalar mass $m_{\pm} > 90 \text{ GeV}$ [35]. Following the recent LHC exclusion of SM-like Higgs masses in the region 127–600 GeV [29]-[32], we restrict m_h to the window 115–130 GeV, with special attention to the currently favored value $m_h \cong 126 \text{ GeV}$.

3. METHODOLOGY

In this work we employ the Landau-gauge one-loop finite-temperature effective potential similar to that described in ref. [28], which considered the most general two-Higgs doublet potential. It has the zero-temperature one-loop corrections and counterterms to insure that tree-level mass and VEV relations are preserved, and includes contributions from the scalars, vectors, Goldstone bosons, and the top quark. It further implements resummation of thermal masses.

As in [28], we search the full parameter space of the model using a Markov chain Monte Carlo (MCMC). Models are chosen in such a way as to favor those with large values of (v_c/T_c) , the ratio of the Higgs VEV to the critical temperature, which is the figure of merit for a strong electroweak phase transition, for the purposes of electroweak baryogenesis (see ref. [36] for a review). In addition, we favor models with small values of λ_{DM} , the effective coupling of the DM to the Higgs boson,

$$\lambda_{DM} = (\lambda_1 + \lambda_2 + 2\lambda_3) \quad (3)$$

since this is required by the XENON100 direct detection constraint (see below). Therefore we bias the MCMC using the combination $a \equiv (v_c/T_c)/\lambda_{DM}$, which is designed to produce chains of models such that the probability distribution dP/da , treating the chain as a statistical ensemble, goes like a . We took the random step size for each of the free parameters of the potential to be $\sim 10\%$ of their starting values, determined by a seed model that satisfied the constraints enumerated next.

We implemented the relevant phenomenological and consistency constraints as in [28], namely precision electroweak observables (EWPO), collider mass bounds as described in section 2.1, vacuum stability, and the absence of Landau poles below 2 TeV (an arbitrary cutoff, but sufficient for considering the model to be a valid effective theory up to reasonably high energies).

For the present study, we add to the above criteria the requirement of the correct thermal relic density of dark matter. The relic abundance of a dark matter particle H is given by [37, 38]

$$\Omega_H h^2 \approx \frac{3 \times 10^{-27} \text{ cm}^3 \text{ s}^{-1}}{\langle \sigma v \rangle} = 0.1123 \pm 0.0035 \quad (4)$$

Depending on the DM mass m_{DM} , different annihilation channels contribute to the thermally averaged annihilation cross section. Here we consider $m_{DM} < m_W$ so that the only relevant annihilation channels are those which are mediated by the SM-like Higgs boson into final state $f\bar{f}$ pairs (excluding the top quark). Specifically, we consider the dark matter mass window 45–80 GeV (to be justified by the results below), and the annihilation cross section

$$\langle \sigma v \rangle = \sum_f \frac{3\lambda_{DM}^2 m_f^2}{4\pi ((4m_{DM}^2 - m_h^2)^2 + \Gamma_h^2 m_h^2)} \quad (5)$$

where $m_{DM} = m_H$, $\Gamma_h \cong 0.003 \text{ GeV}$ is the decay width of the Higgs boson (at $m_h \cong 126 \text{ GeV}$), λ_{DM} is given by (3), and the sum is over all kinematically accessible SM fermions, thus dominated by $b\bar{b}$ pairs in the final state.

In addition to the WMAP constraints on relic density, there is also a strict limit on the spin-independent dark matter-nucleon cross section coming from direct detection experiments, notably XENON100 [39]-[41]. The relevant cross section in the present model is given by [12]

$$\sigma_{SI} = \frac{\lambda_{DM}^2 f^2}{4\pi} \frac{\mu^2 m_n^2}{m_h^4 m_{DM}^2} \quad (6)$$

where $\mu = m_n m_{DM}/(m_n + m_{DM})$ is the DM-nucleon reduced mass. The Higgs-nucleon coupling f is subject to hadronic uncertainties that have been discussed in refs. [42, 43], and more recently in [44]; in particular the quark matrix element $\sigma_{\pi N}$ upon which f depends is poorly determined. Many authors take $f \sim 0.35$; for example DarkSUSY [45] uses $f = 0.38$, while ref. [46] finds $f = 0.35$ and a recent estimate based on lattice gauge theory [47] obtains $f = 0.32$ [47]. These do not reflect the full range of possible values, which ref. [44] puts at $f = 0.26 - 0.63$, corresponding to a factor of 6 uncertainty in the direct detection cross section. We adopt the median value $f = 0.35$ for definiteness, but one might reasonably invoke $f = 0.26$ to weaken the effect of direct detection limits (by a factor of 1.8 in the cross section) and thus the degree of fine-tuning of model parameters that we will find below.

Because the same Feynman diagram is responsible for both processes (5) and (6), the XENON100 constraint restricts λ_{DM} to be small. Thus to get a large enough annihilation cross section (5), we must be somewhat close to the resonance condition $m_{DM} \cong m_h/2$, and the model thus requires some moderate tuning. We will quantify this below. The XENON100 90% c.l. limit is $\sigma_{SI} \lesssim 8 \times 10^{-45} \text{ cm}^2$ in the DM mass range of interest, assuming that $m_h \cong 126 \text{ GeV}$.

One further condition we impose is that invisible decays of the SM Higgs boson $h \rightarrow HH$ do not dominate its width, where the invisible contribution is given by

$$\Gamma_{\text{inv}} = \frac{\lambda_{DM}^2 v^2}{64\pi m_h} \sqrt{1 - 4m_{DM}^2/m_h^2} \quad (7)$$

with SM Higgs VEV $v = 246 \text{ GeV}$. Ref. [48] indicates that a constraint at the level of 40% on the branching ratio for such decays should be attainable in the relatively near future from LHC data. Although not yet established, it seems unlikely that the invisible decays dominate the width of the Higgs if the excess events seen at LHC are really due to the Higgs, so we provisionally impose the 40% constraint. Below we will show that this requirement restricts the range of allowed m_{DM} , but only slightly more than the combination of relic density and direct detection constraints.

We also explore a generalization of the above scenario, in which the H boson could make a subdominant contribution Ω_H to the total dark matter density. This will occur if λ_{DM} is larger, for a given value of m_{DM} , than what is required to satisfy (4). The constraint on σ_{SI} from direct detection is correspondingly weakened since the rate goes like $\Omega_H \sigma_{SI} \sim \sigma_{SI}/\langle\sigma v\rangle$. The factors of λ_{DM} cancel out and thus the combined constraints become independent of λ_{DM} so long as it is large enough to sufficiently suppress the relic density.

4. MONTE CARLO RESULTS

We initially performed a MCMC scan of the full model parameter space (varying $\lambda_1, \lambda_2, \lambda_3, \lambda_S, m_1^2$) as described above, without imposing any constraints upon the relic density or direct detection cross section. We find in this way many models that satisfy the sphaleron constraint $v_c/T_c > 1$ on the ratio of the Higgs VEV to the critical temperature. These results are illustrated in fig. 1 which plots the DM relic density versus SM-like Higgs mass m_h for the models with a strong phase transition (black points). It can be seen that there are many such examples within the mass window $m_h = 115 - 130 \text{ GeV}$, as well as within the 3σ allowed range $\Omega h^2 \in [0.085, 0.139]$ for the relic density as determined by Seven-Year Wilkinson Microwave Anisotropy Probe (WMAP) observations [38], and indicated by the shaded horizontal band. A fraction of the points also satisfy the XENON100 constraint; these are denoted by blue crosses. A small population can be found that simultaneously satisfy both constraints

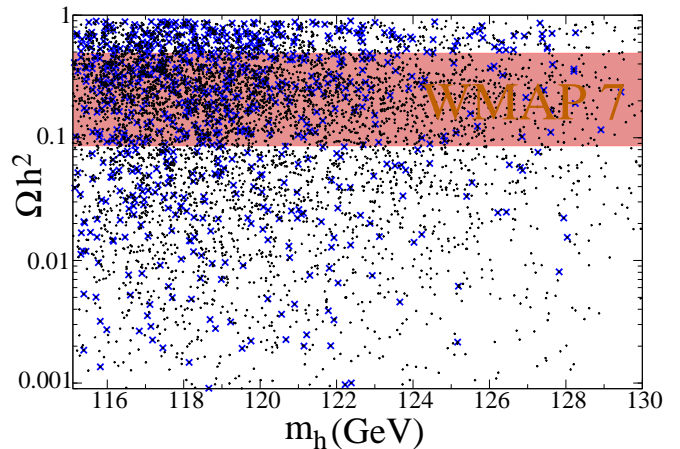


FIG. 1: Scatter plot of dark matter relic density Ωh^2 versus Higgs mass m_h from Monte Carlo, for models with a strong first order electroweak phase transition ($v_c/T_c > 1$). Dense points (black) correspond to models that do not necessarily satisfy the XENON100 constraint, while crosses (blue) indicate models that do. The shaded band corresponds to relic density $\Omega h^2 \in [0.085, 0.139]$ observed by WMAP at 3σ .

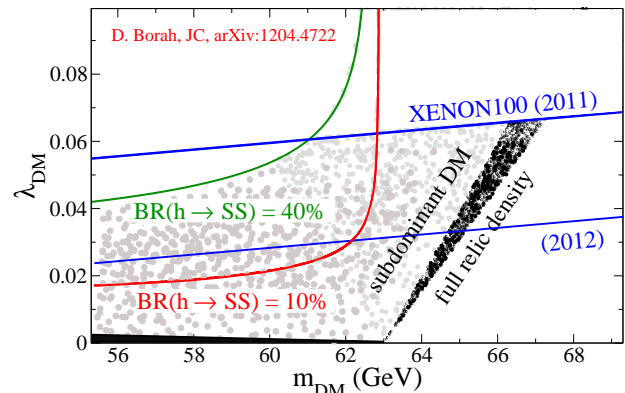


FIG. 2: Scatter plot of λ_{DM} versus m_{DM} for models with strong EWPT, correct relic density (dark points), and $m_h = 126 \text{ GeV}$. The 90% c.l. upper bounds on λ_{DM} from XENON100 (2011) [40] and (2012) [41] are shown by the slanted lines. The light shaded points denote models whose relic density is subdominant, $\Omega_H h^2 < 0.085$, but which still satisfy the correspondingly relaxed XENON100 limit. The other curves indicate the upper limit on λ_{DM} from requiring that the branching ratio for the invisible decay $h \rightarrow HH$ not exceed 10% or 40%, respectively.

and which have m_h near 126 GeV. We use these as seeds for a more focused MCMC search in which only models with the correct relic density and small enough direct detection cross section are admitted into the chains.

Highlighting the effect of the direct detection constraint, figure 2 shows the scatter plot of MCMC models

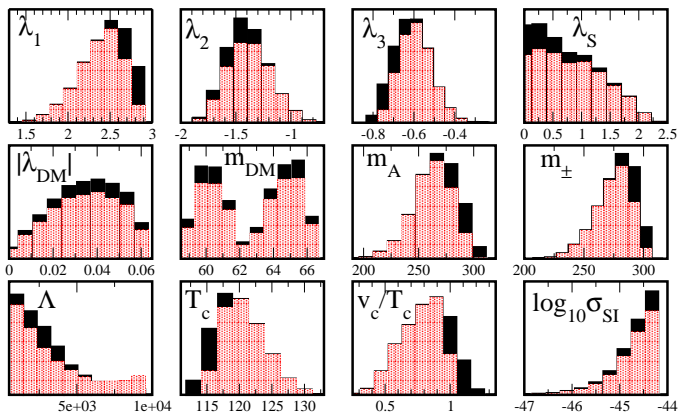


FIG. 3: Monte Carlo distributions of model parameters and derived quantities satisfying all constraints (including $\Omega_H h^2 \in [0.085, 0.139]$), with m_h fixed at 126 GeV. Light-shaded regions indicate the proportion of frequency contributed by models with $v_c/T_c < 1$, while dark corresponds to $v_c/T_c > 1$. Λ is the energy scale of the Landau pole for each model. Masses, Λ and the critical temperature T_c are in GeV units. The spin-independent DM-nucleon scattering cross section σ_{SI} is in units of cm^2 .

having $v_c/T_c > 1$ and correct relic density,¹ in the plane of λ_{DM} versus m_{DM} for the case of $m_h = 126$ GeV which is suggested by the recent results from the ATLAS and CMS experiments. The XENON100 upper limit on λ_{DM} is plotted as the slanting line. The peculiar V-shape of the allowed region is due to the need for being close to resonance of the virtual Higgs boson in the s -channel to get sufficiently strong annihilation for the relic abundance. Larger values of λ_{DM} do not require m_{DM} to be as close to $m_h/2$. The different density of points above and below the Xenon constraint is due to using a rough, preliminary MCMC to find the former points, and the more focused search to find the latter.

We also show in fig. 2 the upper limits on λ_{DM} from requiring that the branching ratio for the invisible decays $\text{BR}(h \rightarrow HH)$ not exceed 40% or 10% respectively. These are futuristic requirements, but ref. [48] estimates that the 40% limit will be attainable with 20 fb^{-1} of integrated luminosity at the LHC. When combined with the allowed region in our plot this constraint leads to the lower bound $m_{DM} \gtrsim 60$ GeV. This is only slightly more stringent than the bound due to direct detection on the left arm of the “V”. The interior region of the “V” is populated by models for which H makes a subdominant contribution to the relic density. In this sample, the con-

straint on the invisible width of the Higgs can be more important than the XENON100 constraint, over a wider range of H masses.

A summary of the favored values of the Lagrangian parameters, mass spectra, and EWPT and DM attributes, from the refined MCMC search implementing all constraints (assuming H accounts for all of the DM and not just a subdominant component), is given by the histogram plots of fig. 3, where the light-shaded portions of the bars indicate the fraction of models in the chain having $v_c/T_c < 1$ for the given parameter value, while the dark shaded part shows the proportion contributed by models with $v_c/T_c > 1$. The chain contains 14400 models, of which 2400 have $v_c/T_c > 1$, despite the biasing of the MCMC toward large values of v_c/T_c . This shows that obtaining a strong first order EWPT is not altogether easy.

Another striking feature is that λ_1 is always large for the cases with $v_c/T_c > 1$, in the range 2.6–3. One might expect such large couplings to cause a breakdown of perturbation theory. Nevertheless we have run the renormalization group equations up to find the Landau pole energy scale Λ in each case, keeping only those models with $\Lambda > 2$ TeV. The values of Λ for our accepted models are in the range 2–5 TeV; thus some additional new physics must come into play at these higher energies.

A consequence of the large values of λ_1 and $|\lambda_2|$ is that there must be fine-tuning between λ_1 and the combination $\lambda_2 + 2\lambda_3$ at the level of $(1.4 \pm 0.5)\%$ (the minimum level of tuning we find is 2.5% among the models in our chain with $v_c/T_c > 1$) in order to make λ_{DM} sufficiently small. As we noted above, there is an additional tuning between $2m_{DM}$ and m_h , which we find to be at the level of $(3.7 \pm 1.4)\%$ in the $v_c/T_c > 1$ subsample. The fine-tuning problem for λ_{DM} is slightly ameliorated in the scan of models having $\Omega_H h^2 < 0.085$, for which we find that $\lambda_2 + 2\lambda_3$ must cancel λ_1 at the level of $3.8 \pm 2.7\%$, a factor of 3 improvement.

5. IMPLICATIONS FOR LHC

The IDM presents a challenge for discovery at collider experiments. From fig. 3, we see that the masses of the CP-odd and charged Higgs bosons A and H^\pm are predicted to be in a relatively narrow window 260–320 GeV. We find that there is no strong correlation between m_A or m_\pm and m_{DM} , but there is a noticeable correlation (due to the EWPO constraint) between m_\pm and m_A , shown in fig. 4. The allowed region consistent with $v_c/T_c > 1$ and H providing the dominant DM component is shown by the dark crosses in the upper part of the region of interest. This gets extended to somewhat smaller masses for the case of models where H is a subdominant DM component.

Because the inert doublet does not couple to quarks, its production cross section is suppressed relative to that of the SM Higgs, proceeding mainly by $q\bar{q} \rightarrow (A, H)$,

¹ We have corrected fig. 2 since the original submission by approximately taking into account the effect of thermal averaging, not done in eq. (5), which is the cross section in the limit of zero velocity. Thermal averaging allows for some fraction of DM with $m_{DM} < m_h/2$ to cause resonant annihilation and so significantly suppresses the relic density relative to using eq. (5) in these cases.

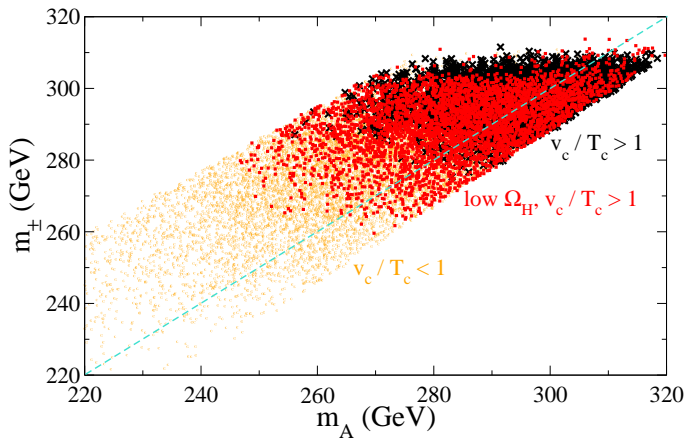


FIG. 4: Scatter plot of charged Higgs mass m_{\pm} versus CP-odd Higgs mass m_A , for models satisfying all constraints. Dark-shaded upper region (crosses): models with $v_c/T_c > 1$; lighter-shaded middle region (squares): models with subdominant DM component $\Omega_H h^2 < 0.085$ but $v_c/T_c > 1$; lightest-shaded lower region (dots): models with $v_c/T_c < 1$. The diagonal line shows where $m_{\pm} = m_A$.

(H^{\pm}, H^{\mp}), (H^{\pm}, A) or (H^{\pm}, H) through a virtual Z or W in the s channel. Ref. [19] argues that a promising discovery signal is through the subsequent decay of the heavy Higgs boson(s) to produce lepton pairs and missing energy. However the models shown to be most favorable for discovery with 100 fb^{-1} of integrated luminosity are those with $|m_A - m_{DM}| \sim 40 - 80 \text{ GeV}$ or $m_{DM} \sim 40 \text{ GeV}$, which do not include the ones we predict in the present analysis. A similar conclusion holds for the trilepton discovery channel [23].

Ref. [49] more generally considers monojet events induced by dimension 6 operators of the form $\bar{q}q\bar{\chi}\chi/\Lambda^2$ for Dirac DM χ coupling to quarks, producing a jet from initial state radiation of a gluon from a quark, as well as missing energy from the DM. The IDM generates such operators with a virtual Z boson at one loop, through the $ZZHH$ coupling, leading to a dimension 6 operator of order $(G_F/96\pi^2)\bar{q}\vec{\partial}q|H|^2$. Even though the effective description is not valid at LHC energies, it should give an upper bound on the strength of this virtual process. Due to the initial state radiation, one of the quarks is off-shell, so $\vec{\partial}$ will be of order the momentum of the jet rather than the quark mass. Even so, we find that the $\bar{q}\vec{\partial}q|H|^2$ operator produces an amplitude similar to that of $\bar{q}q\bar{\chi}\chi/\Lambda^2$ with $\Lambda \sim 7 \text{ TeV}$, which is far beyond the current sensitivity of LHC experiments, $\Lambda > 700 \text{ GeV}$, determined by ref. [49]. The mismatch arises because of the loop suppression factor in our model. The monojet constraint is more stringent for operators generated by tree-level exchange. For the IDM, the most important such process is $q\bar{q} \rightarrow HA$ via s -channel Z exchange, followed by $A \rightarrow HZ$. Hadronic decays $Z \rightarrow q\bar{q}H$ could then appear as monojets plus missing energy, if the Z is sufficiently boosted so that only one jet is resolved. It

could be interesting to undertake a study of such processes tailored to the IDM.

Another possibility for testing the IDM is by the effect of the charged Higgses on the $h \rightarrow \gamma\gamma$ branching ratio [21, 26]. The rate for $h \rightarrow \gamma\gamma$ is given by

$$\Gamma = \frac{G_F \alpha^2 m_h^3}{128 \sqrt{2} \pi^3} |A_{SM} + A_{H^{\pm}}|^2 \quad (8)$$

where $A_{SM} = -6.52$ for $m_h = 126 \text{ GeV}$ and

$$A_{H^+} = -\frac{\lambda_1 v^2}{2m_{\pm}^2} (\tau^{-1} - \tau^{-2} (\sin^{-1} \sqrt{\tau})^2) \cong \frac{1}{3} \quad (9)$$

with $\tau = (m_h/2m_{\pm})^2$. The approximation $A_{H^+} \cong 1/3$ holds in the limit $m_{\pm} \gg m_h$ and $\lambda_1 v^2 \cong 2m_{\pm}^2$ which are satisfied in the models favored by our analysis. Therefore the H^{\pm} contribution interferes destructively with that of the SM, and results in a increase close to 10% in the $h \rightarrow \gamma\gamma$ partial width for all the models that we consider. However there is a larger effect on the branching ratio for $h \rightarrow \gamma\gamma$ due to the invisible decay channel $h \rightarrow HH$, which increases the total decay width relative to that in the standard model. Thus the change in the branching ratio $\text{BR}(h \rightarrow \gamma\gamma)$ may be dominated by the dilution due to $h \rightarrow HH$ in the region where $m_H < m_h/2$. If on the other hand $m_H > m_h/2$, we have the definite prediction that $\text{BR}(h \rightarrow \gamma\gamma)$ is close to 90% of its standard model value. Such a reduction is in the opposite direction of the upward fluctuation in the value that was previously observed by CMS [30].

6. CONCLUSIONS

We have quantitatively reconsidered the impact of an inert Higgs doublet on the strength of the electroweak phase transition, generally confirming the result of ref. [27] that it is relatively easy to find models satisfying all constraints and giving $v_c/T_c > 1$, but we differ in the details. Whereas ref. [27] finds allowed masses $m_{\pm} \cong m_A$ in the range $280 - 370 \text{ GeV}$, we find a more restricted range $260 - 320 \text{ GeV}$, correlated with our limit $\lambda_1 < 3$ in contrast to theirs, $\lambda_1 < 4$. Considering the approximate nature of the finite-temperature effective potential used in [27], the results seem to be in reasonable agreement.

However, we have pointed out some fine-tunings needed to make the scenario work: m_{DM} must be within $\sim 4 \text{ GeV}$ of $m_h/2$ to get a strong enough $HH \rightarrow b\bar{b}$ annihilation cross section for the observed relic density, while the large value of λ_1 needed to get $v_c/T_c > 1$ is canceled typically at the (1-4)% level (depending upon whether H is the dominant component of the total DM density) by $\lambda_2 + 2\lambda_3$ so that the DM-nucleon coupling is small enough to satisfy the XENON100 constraint. If the IDM dark matter plus strong EWPT scenario should be borne out by experiments, it will be mysterious why these two seemingly unlikely coincidences should exist.

We have considered the prospects for testing the scenario at the LHC. There are several possible signatures: invisible decays of the SM-like Higgs into dark matter could be inferred if $m_{DM} \lesssim 61$ GeV. A 10% decrease in the partial width for $h \rightarrow \gamma\gamma$ is a firm prediction. Current analyses of missing energy plus monojets or dileptons do not seem able to rule out the model in the near future, but we suggest for further study that the process $q\bar{q} \rightarrow HA$ followed by $A \rightarrow ZH$ and hadronic decays of the Z (if sufficiently boosted) could give monojet-like events that

might constitute a more promising signal.

Acknowledgements. We thank Mike Trott for his kind assistance in generating EWPO constraints for the mass ranges of interest and for valuable suggestions, and Joel Giedt, Joachim Kopp, Sabine Kraml and Guy Moore for enlightening discussions. The visit of D.B. to McGill University was supported by Canadian Commonwealth Fellowship Program. JC's research is supported by NSERC (Canada).

-
- [1] G. W. Anderson and L. J. Hall, Phys. Rev. D **45**, 2685 (1992).
- [2] S. Dimopoulos, R. Esmailzadeh, L. J. Hall and N. Tetradis, Phys. Lett. B **247**, 601 (1990).
- [3] V. Barger, P. Langacker, M. McCaskey, M. Ramsey-Musolf and G. Shaughnessy, Phys. Rev. D **79**, 015018 (2009) [arXiv:0811.0393 [hep-ph]].
- [4] J. Kang, P. Langacker, T. Li and T. Liu, JHEP **1104**, 097 (2011) [arXiv:0911.2939 [hep-ph]].
- [5] P. Kumar and E. Ponton, JHEP **1111**, 037 (2011) [arXiv:1107.1719 [hep-ph]].
- [6] D. J. H. Chung and A. J. Long, Phys. Rev. D **84**, 103513 (2011) [arXiv:1108.5193 [astro-ph.CO]].
- [7] J. Kozaczk and S. Profumo, JCAP **1111**, 031 (2011) [arXiv:1108.0393 [hep-ph]].
- [8] M. Carena, N. R. Shah and C. E. M. Wagner, Phys. Rev. D **85**, 036003 (2012) [arXiv:1110.4378 [hep-ph]].
- [9] A. Ahriche and S. Nasri, arXiv:1201.4614 [hep-ph].
- [10] M. Gonderinger, H. Lim and M. J. Ramsey-Musolf, arXiv:1202.1316 [hep-ph].
- [11] E. Ma, Phys. Rev. D **73**, 077301 (2006) [hep-ph/0601225].
- [12] R. Barbieri, L. J. Hall and V. S. Rychkov, Phys. Rev. D **74**, 015007 (2006) [hep-ph/0603188].
- [13] D. Majumdar and A. Ghosal, Mod. Phys. Lett. A **23**, 2011 (2008) [hep-ph/0607067].
- [14] L. Lopez Honorez, E. Nezri, J. F. Oliver and M. H. G. Tytgat, JCAP **0702**, 028 (2007) [hep-ph/0612275].
- [15] Q. -H. Cao, E. Ma and G. Rajasekaran, Phys. Rev. D **76**, 095011 (2007) [arXiv:0708.2939 [hep-ph]].
- [16] P. Agrawal, E. M. Dolle and C. A. Krenke, Phys. Rev. D **79**, 015015 (2009) [arXiv:0811.1798 [hep-ph]].
- [17] S. Andreas, M. H. G. Tytgat and Q. Swillens, JCAP **0904**, 004 (2009) [arXiv:0901.1750 [hep-ph]].
- [18] E. Nezri, M. H. G. Tytgat and G. Vertongen, JCAP **0904**, 014 (2009) [arXiv:0901.2556 [hep-ph]].
- [19] E. Dolle, X. Miao, S. Su and B. Thomas, Phys. Rev. D **81**, 035003 (2010) [arXiv:0909.3094 [hep-ph]].
- [20] C. Arina, F. -S. Ling and M. H. G. Tytgat, JCAP **0910**, 018 (2009) [arXiv:0907.0430 [hep-ph]].
- [21] P. Posch, Phys. Lett. B **696**, 447 (2011) [arXiv:1001.1759 [hep-ph]].
- [22] L. Lopez Honorez and C. E. Yaguna, JHEP **1009**, 046 (2010) [arXiv:1003.3125 [hep-ph]].
- [23] X. Miao, S. Su and B. Thomas, Phys. Rev. D **82**, 035009 (2010) [arXiv:1005.0090 [hep-ph]].
- [24] A. Melfo, M. Nemevsek, F. Nesti, G. Senjanovic and Y. Zhang, Phys. Rev. D **84**, 034009 (2011) [arXiv:1105.4611 [hep-ph]].
- [25] C. Arina and N. Sahu, Nucl. Phys. B **854**, 666 (2012) [arXiv:1108.3967 [hep-ph]].
- [26] A. Arhrib, R. Benbrik and N. Gaur, arXiv:1201.2644 [hep-ph].
- [27] T. A. Chowdhury, M. Nemevsek, G. Senjanovic and Y. Zhang, JCAP **1202**, 029 (2012) [arXiv:1110.5334 [hep-ph]].
- [28] J. M. Cline, K. Kainulainen and M. Trott, JHEP **1111**, 089 (2011) [arXiv:1107.3559 [hep-ph]].
- [29] G. Aad *et al.* [ATLAS Collaboration], Phys. Lett. B **710**, 49 (2012) [arXiv:1202.1408 [hep-ex]].
- [30] S. Chatrchyan *et al.* [CMS Collaboration], arXiv:1202.1488 [hep-ex].
- [31] S. Chatrchyan *et al.* [CMS Collaboration], arXiv:1202.1487 [hep-ex].
- [32] G. Aad *et al.* [ATLAS Collaboration], Phys. Rev. Lett. **108**, 111803 (2012) [arXiv:1202.1414 [hep-ex]].
- [33] M. Cirelli, N. Fornengo, and A. Strumia, Nucl. Phys. **B753**, 178 (2006), hep-ph/0512090.
- [34] E. Lundstrom, M. Gustafsson, and J. Edsjo, Phys. Rev. **D79**, 035013 (2009), 0810.3924.
- [35] A. Pierce and J. Thaler, JHEP **0708**, 026 (2007) [hep-ph/0703056 [HEP-PH]].
- [36] J. M. Cline, "Baryogenesis," lectures given at Les Houches Summer School 2006, hep-ph/0609145.
- [37] G. Jungman, M. Kamionkowski, and K. Griest, Phys. Rept. **267**, 195 (1996), hep-ph/9506380.
- [38] N. Jarosik *et al.*, Astrophys. J. Suppl. **192**, 14 (2011), 1001.4744.
- [39] E. Aprile *et al.* (XENON100), Phys. Rev. Lett. **105**, 131302 (2010), 1005.0380.
- [40] E. Aprile *et al.* [XENON100 Collaboration], Phys. Rev. Lett. **107**, 131302 (2011) [arXiv:1104.2549 [astro-ph.CO]].
- [41] E. Aprile *et al.* [XENON100 Collaboration], Phys. Rev. Lett. **109**, 181301 (2012) [arXiv:1207.5988 [astro-ph.CO]].
- [42] J. R. Ellis, K. A. Olive and C. Savage, Phys. Rev. D **77**, 065026 (2008) [arXiv:0801.3656 [hep-ph]].
- [43] A. Bottino, F. Donato, N. Fornengo and S. Scopel, Phys. Rev. D **78**, 083520 (2008) [arXiv:0806.4099 [hep-ph]].
- [44] Y. Mambrini, Phys. Rev. D **84**, 115017 (2011) [arXiv:1108.0671 [hep-ph]].
- [45] P. Gondolo, J. Edsjo, P. Ullio, L. Bergstrom, M. Schelke and E. A. Baltz, JCAP **0407**, 008 (2004) [astro-ph/0406204].
- [46] J. R. Ellis, A. Ferstl and K. A. Olive, Phys. Lett. B **481**, 304 (2000) [hep-ph/0001005].

- [47] J. Giedt, A. W. Thomas, and R. D. Young, Phys. Rev. Lett. **103**, 201802 (2009), 0907.4177.
- [48] Y. Bai, P. Draper and J. Shelton, arXiv:1112.4496 [hep-ph].
- [49] P. J. Fox, R. Harnik, J. Kopp and Y. Tsai, arXiv:1109.4398 [hep-ph].

